EPJ Web of Conferences **259**, 06001 (2022) https://doi.org/10.1051/epjconf/202225906001
SQM 2021

Global and local polarization of Λ ($\overline{\Lambda}$) hyperons in Pb–Pb collisions in ALICE at the LHC

Debojit Sarkar[1,*] (for the ALICE Collaboration)

[1]Wayne State University, 666 W Hancock St, Detroit, MI-48201, USA

Abstract. The global polarization of the Λ and $\overline{\Lambda}$ hyperons ($P_{\rm H}$) has been measured in Pb–Pb collisions at $\sqrt{s_{\rm NN}}$ = 2.76 TeV and 5.02 TeV in ALICE at the Large Hadron Collider (LHC). The hyperon global polarization is found to be consistent with zero at both collision energies. The local polarization of the Λ and $\overline{\Lambda}$ hyperons along the beam (z) direction, $P_{\rm z}$, has also been measured in Pb–Pb collisions at $\sqrt{s_{\rm NN}}$ = 5.02 TeV. The $P_{\rm z}$, measured as a function of the hyperon emission angle relative to the second harmonic symmetry plane, exhibits a second harmonic sine modulation, as expected due to elliptic flow. The measurements of global and local hyperon polarization are reported for different collision centralities and as a function of transverse momentum in semicentral collisions. These results show the first experimental evidence of a non-zero hyperon $P_{\rm z}$ in Pb–Pb collisions at the LHC.

The initial large orbital angular momentum of the colliding nuclei in a relativistic non-central nucleus–nucleus collision might be partially transferred to the system created in such collision [1]. This system, known to behave almost like an ideal fluid [2], would exhibit a vortical behavior with vorticity on average directed perpendicular to the reaction plane defined by the impact parameter vector and the beam direction. Due to spin-orbit interactions, all emitted final state particles may become polarized along the system's orbital angular momentum, the phenomenon termed as global polarization [1, 3, 4]. As the spin of a particle cannot be measured directly, the parity violating weak decays of $\Lambda \to {\rm p} + \pi^-$ and $\overline{\Lambda} \to \overline{\rm p} + \pi^+$ in which the momentum of the daughter (anti)proton is correlated with the spin of the hyperon, are used to measure the polarization in the system. The polarization vector $P_{\rm H}$ generally depends on the hyperon kinematics, namely the transverse momentum $p_{\rm T}$, rapidity $y_{\rm H}$, and its azimuthal angle with respect to the reaction plane, $\varphi - \Psi_{\rm RP}$, as well as the collision centrality [5]

$$P_{\rm H}(p_{\rm T}, y_{\rm H}, \varphi) = -\frac{8}{\pi\alpha_{\rm H}}\langle \sin(\varphi^*_{\rm p} - \Psi_{\rm RP})\rangle, \tag{1}$$

where $\varphi^*_{\rm p}$ is the azimuthal angle of the (anti)proton direction in the hyperon rest frame and α_H is the hyperon decay parameter [6]. The reaction plane angle $\Psi_{\rm RP}$ is estimated using the spectator plane angle $\Psi_{\rm SP}$, characterizing the deflection direction of the spectator neutrons [5]. In addition to the vorticity due to the orbital angular momentum of the entire system, other physics processes, such as anisotropic flow, jet energy deposition, deviation from longitudinal boost invariance of the transverse velocity fields, generate vorticity along different directions depending on the location of the fluid elements in the created system [7–10]. In particular, in non-central nucleus-nucleus collisions, the strong elliptic flow would generate a non-zero

*e-mail: debojit.sarkar@cern.ch

vorticity component along the beam axis (z) [8, 9]. The vorticity and the corresponding polarization exhibits a quadrupole structure in the transverse plane. This polarization can be characterized by the second harmonic sine component in the Fourier decomposition of the polarization along the beam axis (P_z) as a function of the particle azimuthal angle relative to the second harmonic symmetry plane [11]

$$P_{z,s2} = \langle P_z \sin(2\varphi - 2\Psi_2)\rangle, \tag{2}$$

$$P_z(p_T, y_H, \varphi) = \frac{\langle \cos\theta_p^*\rangle}{\alpha_H \langle(\cos\theta_p^*)^2\rangle}, \tag{3}$$

where θ_p^* is the polar angle of the (anti)proton direction in the hyperon rest frame and Ψ_2 is the second harmonic symmetry plane angle. The factor $\langle(\cos\theta_p^*)^2\rangle$ serves as a correction for finite acceptance along the longitudinal direction. The sign of $P_{z,s2}$ determines the phase of the P_z modulation relative to the second harmonic symmetry plane.

The analyzed data samples were recorded by ALICE in 2010 and 2011 for Pb–Pb collisions at $\sqrt{s_{NN}}$ = 2.76 TeV, and in 2015 and 2018 at $\sqrt{s_{NN}}$ = 5.02 TeV [5, 11]. The centrality is determined using the sum of the charge deposited in the V0A ($2.8 < \eta < 5.1$) and the V0C ($-3.7 < \eta < -1.7$) scintillators [5, 11]. After removing the pile up contributions, events that pass central, semi-central, or minimum-bias trigger criteria with a z-component of the reconstructed event vertex (V_z) within ±10 cm are selected. The Λ and $\overline{\Lambda}$ hyperons are reconstructed inside the Time Projection Chamber (TPC) using the decay topology of $\Lambda \to p + \pi^-$ and $\overline{\Lambda} \to \overline{p} + \pi^+$ (64% branching ratio) [12] as described in Ref. [13]. The daughter tracks are assigned the identity of a pion or a (anti)proton based on the charge and particle identification using the specific energy loss (dE/dx) measurement in the TPC. The tracks of the daughter pions and (anti)protons are selected within the pseudorapidity range of $|\eta| < 0.8$ inside the TPC. The Λ and $\overline{\Lambda}$ candidates having invariant mass M_{inv} within the interval 1.103 –1.129 GeV/c^2 with $p_T > 0.5$ GeV/c and $|y_H| < 0.5$ are considered in this measurement [5, 11].

The event-plane method is used for the polarization measurement [14]. The spectator plane angle (Ψ_{SP}) is reconstructed with a pair of neutron Zero Degree Calorimeter (ZDC) detectors [5]. The second harmonic event plane angle (Ψ_2) is reconstructed using the TPC tracks and signals in the V0A and V0C scintillators [11]. A recentering procedure [14] is applied run-by-run as a function of the event centrality, event vertex position (V_x, V_y, V_z), and duration of the run in order to compensate for various effects (e.g., imperfect detector acceptance, varying beam conditions) [5, 11].

The P_H and $P_{z,s2}$ are measured using the invariant mass method [5, 11] by calculating $Q = \langle \sin(\varphi_p^* - \Psi_{SP})\rangle$ for global and $Q = \langle \cos\theta_p^* \sin(2\varphi - 2\Psi_2)\rangle$ for local polarization for all hyperon candidates as a function of the invariant mass and fitting it with the expression

$$Q(M_{inv}) = f^S(M_{inv})Q^S + f^{BG}Q^{BG}(M_{inv}), \tag{4}$$

where f^S and $f^{BG} = 1 - f^S$ are the signal and background fraction of the Λ ($\overline{\Lambda}$) candidates estimated from the invariant mass yields, respectively. The parameter Q^S estimates the signal and $Q^{BG}(M_{inv})$ estimates the possible contribution from the combinatorial background of Λ ($\overline{\Lambda}$) hyperons in the measured polarization. Figure 1 shows the measured hyperon global polarization (P_H) as a function of centrality in Pb–Pb collisions for two collision energies [5]. The P_H at the LHC is found to be consistent with zero within the experimental uncertainties for all studied centrality classes. No signal was observed as a function of rapidity or p_T either [5]. Recent measurements at RHIC show a significant global polarization of Λ and $\overline{\Lambda}$ hyperons in Au–Au collisions at $\sqrt{s_{NN}}$ = 7.7 – 200 GeV with the polarization magnitude monotonically decreasing with increasing $\sqrt{s_{NN}}$ [15, 16]. The decrease in the P_H at

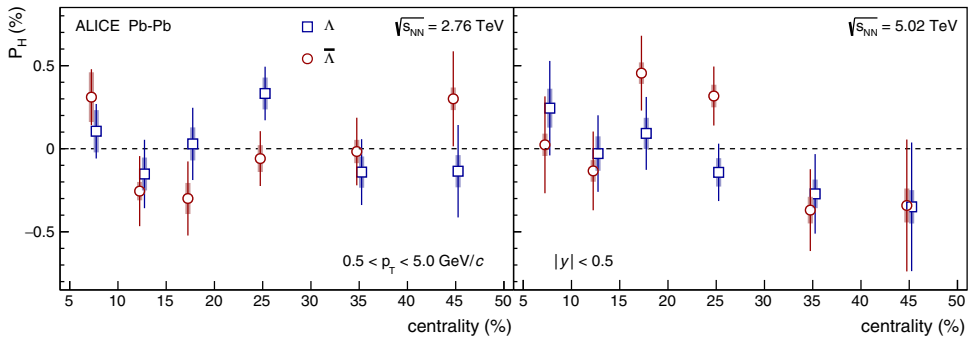

Figure 1. (color online) The global hyperon polarization (P_H) as function of centrality for Pb–Pb collisions at $\sqrt{s_{NN}}$ = 2.76 TeV (left) and 5.02 TeV (right) [5].

midrapidity with collision energy is usually attributed to a decreasing role of the baryon stopping [17] in the initial velocity distributions. The ALICE measurements are consistent with hydrodynamical model calculations for the LHC energies and empirical estimates based on the collision energy dependence of the directed flow due to the tilted source [1, 8, 18].

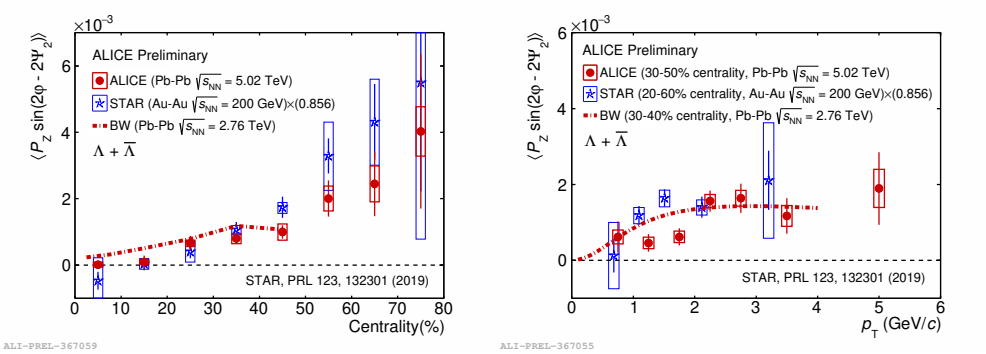

Figure 2. (color online) Centrality dependence of $\langle P_z \sin(2\varphi - 2\Psi_2)\rangle$ averaged for Λ and $\overline{\Lambda}$ in Pb–Pb collisions at $\sqrt{s_{NN}}$ = 5.02 TeV and it's comparison with the RHIC results in Au–Au collisions at $\sqrt{s_{NN}}$ = 200 GeV. The Blast-Wave model calculations [19] for Pb–Pb collisions at $\sqrt{s_{NN}}$ = 2.76 TeV are shown by dashed-dotted line.

The centrality and p_T dependences of $P_{z,s2}$ in Pb–Pb collisions at $\sqrt{s_{NN}}$ = 5.02 TeV and its comparison with the STAR measurements in Au–Au collisions at $\sqrt{s_{NN}}$ = 200 GeV [20] are shown in Fig. 2. The $P_{z,s2}$ decreases towards more central collisions, similar to the elliptic flow. For centralities larger than 60%, the large uncertainties prevent a firm conclusion on the exact mature of its centrality dependence [11]. The $P_{z,s2}$ also shows an increase with p_T up to $p_T \approx 2.0$ GeV/c. For $p_T > 2.0$ GeV/c, the data is consistent with being constant but the uncertainty in the measurement does not allow for a strong conclusion. As the STAR results were obtained with $\alpha_H = 0.642$ whereas the ALICE measurement uses updated values $\alpha_H = 0.750$ (Λ) and -0.758 ($\overline{\Lambda}$), the STAR results are rescaled with a factor 0.856 for a proper comparison [11]. The $P_{z,s2}$ in Pb–Pb collisions at $\sqrt{s_{NN}}$ = 5.02 TeV is similar in magnitude for the central collisions with somewhat smaller value in the semi-

central collisions and has same sign compared to the top RHIC energy. At lower transverse momenta ($p_T < 2.0$ GeV/c), $P_{z,s2}$ at the LHC is smaller than that at the top RHIC energy as shown in the right panel of Fig. 2. The $P_{z,s2}$ does not exhibit a significant dependence on rapidity as shown in Ref. [11]. The sign of the $P_{z,s2}$ is positive at both RHIC and the LHC and in disagreement with hydrodynamic and AMPT models estimations accounting only for the thermal vorticity [21, 22]. Surprisingly, a simple Blast-Wave model, which accounts only for the kinematic vorticity, tuned to reproduce transverse momentum spectra, elliptic flow, and femtoscopic radii, describes the ALICE and STAR results reasonably well [16]. However, the recent hydrodynamical calculations of hyperon polarization based on fluid shear and thermal vorticity coupled with additional assumptions on the hadronization temperature or mass of the spin carrier reproduce the experimentally observed positive $P_{z,s2}$ at RHIC and the LHC energies [11, 21, 22]. These studies indicate that longitudinal polarization is sensitive to the hydrodynamic gradients as well as the dynamics of the spin degrees of freedom through the different stages of the evolution of the system created in heavy-ion collisions. The upcoming Run 3 at the LHC will provide much larger data samples for more differential and precision measurements of local and global hyperon polarization and will further constrain the models aiming to explain the vorticity and the particle polarization in heavy-ion collisions.

References

[1] F. Becattini, G. Inghirami, V. Rolando, A. Beraudo, L. Del Zanna, A. De Pace, M. Nardi, G. Pagliara, V. Chandra, Eur. Phys. J. C **75**, 406 (2015), [Erratum: Eur.Phys.J.C 78, 354 (2018)], 1501.04468
[2] P. Braun-Munzinger, V. Koch, T. Schäfer, J. Stachel, Phys. Rept. **621**, 76 (2016), 1510.00442
[3] Z.T. Liang, X.N. Wang, Phys. Rev. Lett. **94**, 102301 (2005), [Erratum: Phys.Rev.Lett. 96, 039901 (2006)], nucl-th/0410079
[4] S.A. Voloshin (2004), nucl-th/0410089
[5] S. Acharya et al. (ALICE), Phys. Rev. C **101**, 044611 (2020), 1909.01281
[6] M. Ablikim et al. (BESIII), Nature Phys. **15**, 631 (2019), 1808.08917
[7] B. Betz, M. Gyulassy, G. Torrieri, Phys. Rev. C **76**, 044901 (2007), 0708.0035
[8] S.A. Voloshin, EPJ Web Conf. **171**, 07002 (2018), 1710.08934
[9] F. Becattini, I. Karpenko, Phys. Rev. Lett. **120**, 012302 (2018), 1707.07984
[10] X.L. Xia, H. Li, Z.B. Tang, Q. Wang, Phys. Rev. C **98**, 024905 (2018), 1803.00867
[11] S. Acharya et al. (ALICE) (2021), 2107.11183
[12] P.A. Zyla et al. (Particle Data Group), PTEP **2020**, 083C01 (2020)
[13] S. Acharya et al. (ALICE), JHEP **09**, 006 (2018), 1805.04390
[14] A.M. Poskanzer, S.A. Voloshin, Phys. Rev. C **58**, 1671 (1998), nucl-ex/9805001
[15] L. Adamczyk et al. (STAR), Nature **548**, 62 (2017), 1701.06657
[16] J. Adam et al. (STAR), Phys. Rev. C **98**, 014910 (2018), 1805.04400
[17] H. Sorge, A. von Keitz, R. Mattiello, H. Stoecker, W. Greiner, Nucl. Phys. A **525**, 95C (1991)
[18] B. Abelev et al. (ALICE), Phys. Rev. Lett. **111**, 232302 (2013), 1306.4145
[19] T. Niida, private communication, 2020. For the description of the Blast-Wave model see [20]
[20] J. Adam et al. (STAR), Phys. Rev. Lett. **123**, 132301 (2019), 1905.11917
[21] F. Becattini, M. Buzzegoli, A. Palermo, G. Inghirami, I. Karpenko (2021), 2103.14621
[22] B. Fu, S.Y.F. Liu, L. Pang, H. Song, Y. Yin (2021), 2103.10403